



HAL
open science

Nanosized zeolites as a gas delivery platform in a glioblastoma model

Clement Anfray, Sarah Komaty, Aurélien Corroyer-Dulmont, Moussa Zaarour, Charly Hélaine, Hayriye Özçelik, Clélia Allieux, Jérôme Toutain, Kamila Goldyn, Edwige Petit, et al.

► To cite this version:

Clement Anfray, Sarah Komaty, Aurélien Corroyer-Dulmont, Moussa Zaarour, Charly Hélaine, et al.. Nanosized zeolites as a gas delivery platform in a glioblastoma model. *Biomaterials*, 2020, 257, pp.120249. 10.1016/j.biomaterials.2020.120249 . hal-02912573

HAL Id: hal-02912573

<https://normandie-univ.hal.science/hal-02912573>

Submitted on 11 Aug 2020

HAL is a multi-disciplinary open access archive for the deposit and dissemination of scientific research documents, whether they are published or not. The documents may come from teaching and research institutions in France or abroad, or from public or private research centers.

L'archive ouverte pluridisciplinaire **HAL**, est destinée au dépôt et à la diffusion de documents scientifiques de niveau recherche, publiés ou non, émanant des établissements d'enseignement et de recherche français ou étrangers, des laboratoires publics ou privés.

Nanosized zeolites as a gas delivery platform in a glioblastoma model

Running headline: Nanozeolites to deliver gases to glioblastoma

Clément Anfray¹, Sarah Komaty², Aurélien Corroyer-Dulmont¹, Moussa Zaarour², Charly Helaine¹, Hayriye Ozcelik¹, Clélia Allieux¹, Jérôme Toutain¹, Kamila Goldyn², Edwige Petit¹, Karim Bordji¹, Myriam Bernaudin¹, Valentin Valtchev², Omar Touzani¹, Svetlana Mintova^{2*}, and Samuel Valable^{1*}

¹Normandie Université, UNICAEN, CEA, CNRS, ISTCT/CERVOxy group, GIP Cyceron, Caen, France.

²Normandie Université, ENSICAEN, UNICAEN, CNRS, Laboratoire Catalyse et Spectrochimie (LCS), 14050 Caen, France.

*Correspondence and requests for materials should be addressed to:

Samuel Valable (samuel.valable@cnrs.fr)

Fax : +33 2 31 47 02 22

GIP CYCERON, Bd H Becquerel, BP 52259

14074 Caen, France

Svetlana Mintova (mintova@ensicaen.fr)

Fax : +33 2 31 45 28 21

LCS, ENSICAEN, CNRS

6, boulevard Maréchal Juin

14050 Caen, France

Abstract

Approaches able to counteract, at least temporarily, hypoxia, a well-known factor of resistance to treatment in solid tumors are highly desirable. Herein, we report the use of nanosized zeolite crystals as hyperoxic/hypercapnic gas carriers for glioblastoma. First, the non-toxic profile of nanosized zeolite crystals in living animals (mice, rats and non-human primates) and in various cell types is presented. Second, the ability of the nanosized zeolites to act as a vasoactive agent for a targeted re-oxygenation of the tumor after intravenous injection is shown. As attested by an MRI protocol, the zeolites were able to increase oxygenation and blood volume specifically within the brain tumor whilst no changes in the healthy- non tumoral brain- were observed. The first proof of concept for the use of metal-containing nanosized zeolites as a tool for vectorization of hyperoxic/hypercapnic gases in glioblastoma is revealed.

Keywords: Glioblastoma, Hypoxia, Nanosized Zeolites, MRI, Vectorization

Introduction

Even with aggressive conventional therapies for the treatment of glioblastoma (GBM), the most lethal primary brain tumor [1], the median survival of patients remains around 15 months [2].

Hypoxia, a feature of numerous solid tumors, including GBM [3], is defined as the disproportion between oxygen supply and oxygen consumption. Hypoxia arises from increased metabolic rate of cancer cells, poorly efficient tumor vascularization and augmented interstitial pressure, leading to poor oxygen diffusion. Hypoxia activates adaptive survival mechanisms in cancer cells which in turn stimulate tumor development [4] and resistance to treatments [5]. Hypoxia is a well-known factor of poor prognosis for GBM [6]. Therefore, there is great need to develop a new approach to increase oxygen pressure selectively into the hypoxic tumor, at least transiently.

Several methods have been proposed to alleviate hypoxia in tumors. Among them, one cites pure oxygen breathing or carbogen (5% CO₂ mixed with 95% O₂) breathing. Nevertheless, the global outcomes were disappointing in terms of sensitization to radiation therapy in GBM [7,8].

Moreover, in rodent models of GBM, through the use of advanced magnetic resonance imaging (MRI), we have shown that carbogen improved the cerebral blood volume (CBV) and the oxygenation in the healthy brain tissue at the expense of the GBM tumor [9].

Because of the atypical structure and organization of the tumor vasculature and the absence of a lymphatic system [10], many nanoparticles (NP) of several chemical natures have been examined as transporters of contrast agents and anti-cancer agents due to their aptitude to specifically reach tumors [11]. Furthermore, numerous NP have been designed to sensitize the tumor to RT. These comprise gadolinium-containing NP which rely on the Auger effect [12], NP that decrease the self-repair of cancer cells following RT [13], NP which protect the healthy tissue by reducing oxidative stress [14], and NP that generate oxygen *in-situ* [15]. Nevertheless,

few NP were developed to locally and selectively carry gases in the tumor. Even if micron-sized particles were recently demonstrated to carry approximately five times more oxygen than human red blood cells, their use to alleviate hypoxia in brain tumors is not satisfactory because of their large diameter [16].

Among nanoparticles, zeolites with their excellent chemical selectivity, large sorption ability and absence of toxicity [17–19], are now more and more considered for biomedical usage [20,21], including cancer therapy [22,23]. Zeolites are crystalline, porous materials made of interconnected TO_4 tetrahedra, where T atoms are represented by Si and Al. They have regular framework structures composed of cages and pores of different sizes and forms [24]. Zeolites have been synthesized at the nanosize scale and stabilized in colloidal suspensions [25]. The ordered pores of the zeolites are able to adsorb and desorb various molecules, which allow them to act as efficient carriers of several gases such as NO, CO_2 and O_2 [18,26]. The tunable chemical composition of these crystalline materials allows them to adapt to different chemical environments and thus to display an important stability in acidic and alkaline media. Moreover, adding different metal cations (Fe, Gd) inside the nanosized zeolites can modify their functioning, and therefore significantly rises the interest of zeolite NP as an instrument for imaging [27] and gases carriage [18] applications. Consequently, it is of interest to examine nanosized zeolites as gas transporters to alleviate hypoxia in GBM.

In the present study, in a rodent model of GBM, we provide a proof of concept to precisely carry O_2 and/or CO_2 to tumors through the use of metal-containing nanosized zeolite crystals with FAU-type structure to enhance oxygenation and/or blood volume. Gadolinium (Gd) was introduced into the nanozeolites *via* ion exchange to be administered into the blood circulation and tracked using MRI.

Materials and Methods

Preparation of nanosized faujasite (Na-FAU) type zeolites

Stable suspensions of nanosized zeolite (Na-FAU) were prepared from colloidal precursor solution under hydrothermal conditions as we described earlier [28]. The as-prepared precursor suspension for Na-FAU zeolite was kept at room temperature for 24 h, followed by dehydration using freeze-drying method prior hydrothermal treatment at 50 °C for 26 h. After the hydrothermal treatment, the zeolite nanoparticles were purified by six step centrifuge (24,500 rpm, 45 min) and redispersed in double distilled water till pH of 7.

Ion exchange of nanosized faujasite (Gd-FAU) type zeolites

The purified zeolite suspensions (pH=7) were ion exchanged with gadolinium (III) nitrate hexahydrate ($\text{Gd}(\text{NO}_3)_3 \cdot 6\text{H}_2\text{O}$). 25 mL of $\text{Gd}(\text{NO}_3)_3 \cdot 6\text{H}_2\text{O}$ (3 mM) were added to 5 mL Na-FAU suspension (2.5%). The suspensions were then kept under stirring at room temperature for 1 h and then washed by double distilled water. This procedure was repeated twice to obtain the suspensions of ion-exchanged gadolinium (Gd-FAU) nanosized zeolites; pH=7.

Powder X-ray diffraction (XRD) analysis

Powder samples were measured using a PANalytical X'Pert Pro diffractometer with $\text{CuK}\alpha$ monochromatized radiation ($\lambda = 1.5418 \text{ \AA}$). The samples were scanned in the range of 4-50 °2 θ with a step size of 0.02 °.

Transmission electron microscopy (TEM)

The crystal size, morphology and crystallinity of samples were analyzed by a transmission electron microscopy (TEM) using a JEOL 2010 FEG and a FEI LaB6 TECNAI G2 30UT

operated at 200 kV and 300 kV, respectively. Energy Dispersive Spectrometer (EDS) coupled with both microscopes was employed to analyze the chemical content of the zeolite nanocrystals.

Dynamic light scattering (DLS) and zeta potential analysis

The hydrodynamic diameter of nanosized zeolites in water was quantified through the use of Malvern Zetasizer Nano. The quantifications were carried out on samples after purification with a solid concentration of 1 wt%. Furthermore, the surface charge of nanosized zeolite was examined by assessing the zeta potential value of the same suspensions.

N₂ sorption analysis

N₂ adsorption/desorption isotherms were evaluated by Micrometrics ASAP 2020 volumetric adsorption analyzer. Samples were degassed at 250 °C under vacuum overnight before the evaluation. The external surface area and micropore volume were assessed by alpha-plot method using Silica-1000 (22.1 m² g⁻¹ assumed) as a reference. The micropore and mesopore size distributions of solids were extracted from adsorption branch by the Nonlocal Density Functional Theory (NLDFT) and from the desorption branch using the Barret-Joyner-Halenda (BJH) algorithm, respectively.

In-situ adsorption of CO₂ and O₂ on nanosized zeolites

Powder samples of Na-FAU and Gd-FAU were pressed ($\sim 10^7$ Pa) into self-supported disks (2 cm² area, 20 mg.cm⁻²). Fourier-transform infrared (FTIR) spectra were acquired using a Nicolet 6700 IR spectrometer equipped with a mercury cadmium telluride (MCT) detector and an extended KBr beam splitter. Spectra were recorded in the 400–5500 cm⁻¹ range at 4 cm⁻¹ with 128 scans. The *in situ* was evacuated or flooded with different gases and also heated up to 577 °C. The samples were activated at 225 °C for 2 h under vacuum. Various amounts of CO₂ (at 25

°C) or O₂ (at -196 °C) were incorporated into the cell and maintained in equilibrium for 5 min at the corresponding temperatures before recording each spectrum. The *in situ* IR measurements were performed with pure CO₂ up to 4 Torr and pure O₂ up to 100 Torr. Small doses of these gases were introduced progressively, and saturation was achieved after loading ~50% of the specified quantities. The measurements with carbogen (5% CO₂, 95% O₂) were performed at 80-100 Torr, thus ensuring the presence of higher O₂ and CO₂ quantities than those required to achieve saturation upon adsorbing the gases in pure form. All the spectra were normalized to the sample's mass and plotted as absorbance per gram over the wavelength.

Chemical analyses

The chemical composition of as prepared and ion-exchanged zeolites was determined by inductively coupled plasma (ICP) optical emission spectroscopy using a Varian ICP-OES 720-ES.

Loading of gases in zeolite nanocrystals

Na-FAU and Gd-FAU were loaded with CO₂ and/or O₂ by bubbling of the desired gas into the zeolite suspensions with a flow rate of 80 ml/min for 30 min.

Analysis of oxygen release in aqueous and hypoxic conditions

A hypoxia workstation (*IN VIVO2* 500, 3M) was employed to reach a steady and precise gas content of the atmosphere by replacing O₂ by nitrogen. Phosphate buffered saline (PBS) solution was equilibrated with the gas mix of the hypoxia workstation 1 h before the experiment. A closed reaction vessel containing 12 ml of equilibrated PBS at 37 °C was used, and a dissolved oxygen sensor (SevenGo (Duo) proTM / OptiOxTM, Mettler Toledo) was positioned inside the hypoxia chamber. Before any test, baseline was determined by quantifying the oxygen saturation

for 30 min in the PBS solution within the vessel. Zeolites nanocrystals were then added to the system (500 μ l, 1 wt%) and oxygen dissolved in the PBS solution was quantified continuously for 1 h. The oxygen liberation capacity of as prepared and ion-exchanged nanosized zeolites was compared to oxygen-saturated water (used as control). The oxygen release ability of Na-FAU zeolites nanocrystals was assessed at several levels of O₂ (21, 5, 1 and 0.1% of O₂). To discriminate the amount of O₂ provided by the nanosized zeolites from the oxygen contained in the dispersing solution (pure water), the values were subtracted from those of saturated water alone.

Cell culture

The U87-MG human glioblastoma cell line (ATCC, Manassas, VA, USA), HEK 293 cells (Human Embryonic Kidney cells, ATCC) and bEnd.3 (mouse brain endothelial cells, ATCC) were employed. Cells were maintained in DMEM (Sigma-Aldrich, France) supplemented with 10% fetal bovine serum (Eurobio, France), 2 mM glutamine (Sigma-Aldrich, France) and 100 U/ml penicillin/streptomycin (Sigma-Aldrich, France). Cells were kept in culture at 37 °C with 5% CO₂ and 95% humidity.

Primary culture of cortical neurons, from E15–E16 mouse embryos (Swiss mice; CURB, France) and astrocytes, obtained from neonatal (1 to 3-day-old) mice (Swiss, CURB, France) were prepared as previously described [29].

Cells exposure to zeolite nanocrystals

Cells were exposed to zeolites (Na-FAU and Gd-FAU) during 48 h. Nanosized zeolites were added into the wells at a final concentration of 1, 10, 50 or 100 μ g/ml and. Distilled water was used as reference tests.

Analysis of cell viability

Cells were seeded in 24-wells plates before adding zeolites. The viability of the cells was measured 48 h following the treatment with zeolites nanoparticles using the WST-1 assay (Roche, France).

Analysis of cell cycle

The cell cycle of U87-MG and HEK 293 was analyzed using flow cytometry at several time points after cell treatment with 100 µg/ml zeolite nanoparticles. was determined (Beckman Coulter's Gallios flow cytometer, Beckman Coulter SAS, France). The cell distribution in a given phase of cell cycle was determined using propidium iodide labelling and analyzed through the use of the Kaluza software.

Analysis of genotoxicity

Cells were placed in 24-well plates on coverslips and then exposed to 100 µg/ml of nanosized zeolites during 14, 24 or 48 h. Cells irradiated with X-rays (4 Gy, XRad225Cx, PXi) were used as a positive control. Cells were thereafter fixed in 4% PFA during 1 h at 4 °C.

Immunohistochemistry staining of phospho-histone H2AX and micronuclei was performed as previously described [30]. The following primary antibodies were used: phospho-histone H2AX (ser139) (1/200; Cell Signalling Technology, D175, 2577S) and Alexa-555-conjugated anti-rabbit secondary antibody (1/200; Molecular Probes, A21429). Pictures were acquired on a Leica DMI8 microscope.

Animal studies

All animal studies were performed according to European directive (2010/63/EU) and approved by the Ethics committee (agreement numbers: 12727 and N/02-12-11/25/12-14). The animals

were purchased from the Centre Universitaire de Ressources Biologiques (CURB, A14118015, France). Athymic *nude* rats (250–300 g) were housed in specific pathogen free cages and were fed with γ -irradiated laboratory food. Three marmosets (*Callithrix jacchus*, 285-370g; aged 36-64 months) were employed. Data are reported according to ARRIVE guidelines.

All experimentations were performed on anesthetized animals (isoflurane 1.5-2%; N₂O/O₂70/30%).

Delivery of zeolite nanocrystals

Na-FAU or Gd-FAU nanosized zeolites (100 μ l, 1 wt%) or distilled water were daily injected intraperitoneally in Swiss mice during 5 consecutive days. The body weight of the animals was quantified daily during 1 month.

CO₂-loaded Gd-FAU zeolites (300 μ l, 1 wt%) or distilled water were administered i.v. to Wistar rats (CURB, A14118015, France) and arterial blood samples were taken each 5 min to measure CO₂ partial pressure and the pH (RapidLab 348 analyzer; Siemens, Germany).

Glioblastoma model

The model of GBM used was previously described [31]. Briefly, U87-MG cells (5.10⁴ cells in 3 μ l PBS-glutamine 2mM) were implanted in the striatum of nude rats.

MRI studies

All the MRI examinations were performed on a 7 teslas horizontal magnet (Bruker, Ettlingen). In order to quantify the volume of the tumor, T2-weighted MRI examinations were completed once a week according to the following parameters (RARE, acceleration factor of 8; TR/ TE_{eff}= 5000/62.5 msec; number of experiments (NEX) = 2; 20 contiguous slices; resolution = 0.15×0.15×0.5 mm³). Tumor volumes were calculated using ImageJ.

To track Gd-FAU nanosized zeolites, T1w-FLASH images (TR= 500 ms, TE_{eff}= 10.32 ms; NEX=1; 10 slices; resolution = 0.15×0.15×1.5 mm³) were acquired before and every 2 min after the intravenous injection of 300 µl Gd-FAU zeolite suspension (1 wt%) to tumor bearing rats.

In order to quantify the fractional cerebral blood volume (fCBV), P904[®] (200 µmol.kg⁻¹, Guerbet Research) was used as a contrast agent as previously described [9]. fCBV was calculated before and every 5 min during 1 h following an intravenous administration of 300 µl of gas loaded Gd-FAU (1 wt%). Image analyses were performed through the use of ImageJ software [9].

To measure oxygen saturation (SatO₂) in the brain tissue, we used the BOLD-MRI approach described in our previous article [9]. SatO₂ maps before and after administration of gas loaded Gd-FAU zeolites were obtained in every rat.

Statistical analyses

Data are expressed as mean ± s.d. Statistical analyses were carried out with JMP programs (SAS Institute) and are detailed in each caption.

Results and discussion

Physicochemical characterizations of nanosized zeolites

The main physicochemical properties of Na-FAU zeolite nanocrystals are presented in **Figure 1** and **Table S1 and S2**. Powder X-ray diffraction (XRD) patterns of the zeolite samples contain broad peaks reflecting the small particle size and typical Bragg peaks corresponding to FAU-type zeolite (**Figure 1A**). As quantified by DLS, the nanosized zeolites have an average size of 15-20 nm in water suspension with a concentration of 1% (**Figure 1B**). The zeta potential (ζ) of the zeolite nanocrystals in water suspension is -43 to -45 mV, which corresponds to highly stable negatively surface charged crystals (**Figure 1C**). Porosity of zeolite nanoparticles was analyzed

by N₂ sorption approach (**Figure 1D** and **Table S2**). The data show type I isotherm at low P/P₀, indicative of microporous materials and high adsorption uptake at P/P₀ > 0.8. This shows the high textural mesoporosity of closely packed zeolite nanoparticles with similar particle dimensions.

Na-FAU zeolites with a large supercage (1.1 nm) have been reported as gas carriers [32] and drug delivery systems [22,33]. The adsorption of pure O₂, pure CO₂ and carbogen (95% O₂, 5% CO₂) was examined. The physisorbed O₂ and physisorbed and chemisorbed CO₂ in zeolites were assessed by *in-situ* IR spectroscopy following the incorporation of precise amounts of the desired gases into the zeolite samples (**Figure 2A**). Following the addition of carbogen, the intensity of the band at 2346 cm⁻¹ corresponding to the physisorbed CO₂ (**Table S3**) is similar to that of pure CO₂ (see the experimental section), indicating that the presence of O₂ does not substantially influence the capacity of Na-FAU towards CO₂. On the other hand, the intensity of physisorbed O₂ is lowered by 50% upon using carbogen for loading of zeolites (**Figure 2B**). These results suggest that in the presence of carbogen (O₂ and CO₂), a competition of the two gases on the available cationic sites takes place. The band area corresponding to the adsorbed O₂ decreased which may be related, at least in part, to the low sensitivity of the IR. While the band area corresponding to the adsorbed CO₂ from the pure gas and carbogen is similar due to the same concentration delivered to the sample (see experimental section). Additionally, our theoretical studies showed that a strong affinity of FAU-type zeolites towards O₂, even in the presence of CO₂, is expected [34].

The capacity of zeolites to release the oxygen payload was analyzed in aqueous solutions preliminary equilibrated at various O₂ concentrations in a hypoxic workstation to mimic the oxygen gradients observed in the organism [35] and tumors [36] (**Figure S1**). 5 mg of oxygen-

loaded Na-FAU were introduced in the system and the evolution of oxygen concentration was recorded (**Figure 2C**). Interestingly, the quantity of O₂ released from the Na-FAU zeolites increased as the initial O₂ concentration in the system decreased. Indeed, when the oxygen concentration in the workstation was set at 21%, the oxygen release was 0.6 ± 0.23 mg/ml. When the O₂ concentration was set at 5% (which corresponds to the percentage of O₂ measured in the healthy brain [35]), the release increased to 0.96 ± 0.15 mg/ml. Further, the oxygen release continued increasing to 1.28 ± 0.12 and to 1.5 ± 0.10 mg/ml at 1% and 0.1% of oxygen in the workstation. These oxygen concentrations were chosen to mimic the area of severe hypoxia found in some regions of GBM [36]. More precisely, at 0.1% O₂, addition of 5 mg of Na-FAU zeolite to the system resulted in the delivery of 0.26 mg of oxygen per ml (value deducted from water alone). Based on these experimental results, we calculated that Na-FAU zeolites can transport approximately 19 mmol of O₂/g. To compare with other products developed to deliver oxygen, for example the HEMOXYCarrier®, a natural giant extracellular haemoglobin from polychaete annelids [37] and the Polymer Hollow Microparticles [16] can transport 0.0433 mmol and 0.511 mmol of O₂/g respectively. These experimental results suggest that the lower the external O₂ concentration is, the more zeolites release their O₂ payload. This result reinforces the idea that they could be appropriate gas carriers (CO₂ and/or O₂) to reduce hypoxia in the most hypoxic regions of the tumor.

Evaluation of nanosized zeolites toxicity *in vitro*

Several cell types originating from many organs were exposed to zeolite suspensions with concentrations ranging from 1 to 100 µg/ml for 48 h (**Figure 3A**). DLS analyses of the nanosized zeolites in serum show no aggregation of the nanoparticles (**Figure S2A**). In addition, we conducted further experiments in order to address the stability of zeolites in serum but also in

conditions used to mimic tumor microenvironment (pH = 6.8). Zeolites were diluted at a concentration of 1% in serum and in saline and stored at 37 °C for 9 days. The results are presented in **Figure S2B**. The aspect of the samples did not change with time, no sedimentation was observed, which confirms their stability in these milieu.

U87-MG and primary cell cultures of brain origin were employed to address potential toxicities to the brain tumor and to the surrounding brain cells. We also used an endothelial cell line (bEnd.3) and a kidney cell line (HEK 293) as a reflection of possible systemic toxicities after intravenous injections. No significant toxicity was found for all cell lines and astrocytes (**Figure 3A**). Neurons seemed to be the most sensitive as the maximal loss in cell viability ($65.8 \pm 2.1\%$) was encountered at the concentration of 100 $\mu\text{g/ml}$ of Na-FAU (**Figure 3A**). The introduction of Gd in the zeolite nanocrystals decreased the toxicity to neurons. This may be attributed to the affinity of Na-FAU for calcium in ion exchange process. In neurons' cytosol, it could compete with the neuronal calcium signaling and calcium regulation. When Gd is present in zeolites, the exchange with calcium would be lower, resulting in the reduction of the toxicity. Another explanation would be that the activation of Na/K ATPase in the presence of Na-FAU may enhance potential excitotoxicity processes. To further reinforce this study, the cell cycle was analyzed on U87-MG and HEK 293 by flow cytometry. No difference in the cell distribution at different phases of cell cycle between the control group and cells exposed to nanosized zeolites was observed (**Figure 3B**).

Some reports show, *in vitro*, a genotoxicity of certain types of NP (with a comparable size of about 30 nm) although devoid of cytotoxicity [38]. Therefore, a possible genotoxic action of nanosized zeolites was explored using γH2AX as a marker of DNA double strand breaks and a micronucleus formation assay as a marker of mitotic death. No difference in U87-MG γH2AX

positive cells was observed between control conditions and after exposure to Na-FAU. A slight reduction was observed in the marker after 24 h of experiment in all experimental settings. HEK 293 cells showed a higher number of γ H2AX positive cells in comparison to the U87-MG cells, and the rate of γ H2AX labelled cells was slightly higher at 24 h and 72 h of exposure.

Nevertheless, no difference in the percentage of γ H2AX positive cells after exposure to nanosized zeolites compared to the control condition was detected (**Figure 3C, E**). These findings are also strengthened by the assessment of micronuclei formation. For HEK 293 and U87-MG cells, the amount of cells with micronuclei was less than 10% and was not modified through the time. Moreover, exposure of the cells to the nanosized zeolites did not change the formation of micronuclei. In addition, we found that the presence of Gd did not induce any further toxicity relative to the original Na-FAU zeolites nor further DNA damage (**Figure 3D, E**). Overall, the data indicate that, *in vitro*, nanosized zeolite crystals are devoid of cytotoxicity and genotoxicity on a wide range of cell types.

Evaluation of toxicity of nanosized zeolites in living animals

Although nanoparticles are promising for several clinical applications, their toxicity for living organisms is still a crucial issue. To evaluate the potential adverse actions associated with administrations of nanosized zeolites, studies were performed *in vivo*. First, nanosized zeolites were injected into mice during five successive days, for a total dose of 5 mg per mouse (**Figure 4A**). The body weight curves of mice did not change in comparison to controls. Irrespective of the group and as expected, mice gained 7 g (37% of their initial weight) during the time of the experiment, suggesting no adverse effects of nanosized zeolites on mice.

Though rodent models are helpful to understand the pathophysiology and test treatments of human diseases, more pertinent animal models are necessary to reflect the adverse reactions that

might be displayed in humans. Chiarelli and colleagues proved the importance of employing both rodents and non-human primates for better assessment of the safety of NP [39].

In order to confirm the low toxicity of the nanosized zeolites, the nanosized zeolite suspension (300 μ l, 1 wt%) was injected intravenously to non-human primates (marmoset), and physiological parameters were monitored. A slight decrease in arterial pressure was observed following the injection, from 63 mmHg to 42 mmHg, nevertheless, it was fully reversed in less than 2 min (**Figure 4B**). In addition, blood samples were taken from marmosets. A representative blood analysis is represented for one marmoset (14 years old, male, 350 g) to follow the effects of Na-FAU on blood counts, kidney and liver health of the animal. In order to have general view about the health of animal, whole blood was tested one week before injection (Day -7). Same parameters were tested one hour after injection (Day 0) and one week after injection (Day +7) and are summarized in **Table 1**.

RBC, hemoglobin, hematocrit and platelets values stayed in the normal range during the course of the experiment. Although the measurements of monocytes and eosinophils were found to be in the normal range, the recorded values were close to lower boundary. We observed a slight increase in the number of basophils which may indicate mild allergic reactions. Creatinine and ASAT are commonly measured clinically as part of diagnostic renal and liver function tests respectively. Creatinine concentration along two weeks may show that Na-FAU zeolites have been filtrated/cleared through kidneys. The amount of transaminase also remained in the normal range. Overall, these results clearly demonstrate the absence of acute and chronic toxicity of zeolites nanocrystals applied to living animals.

Post-synthesis modifications of nanosized zeolites and *in vivo* tracking of nanosized zeolites in healthy and tumor bearing rats

We introduced low amount of extra framework gadolinium to track the particles with ICP-MS and MRI. ICP-MS analysis showed that the ion-exchange process resulted in incorporation of 1.24 wt% of Gd in zeolites (Gd-FAU) (**Table S1**). The presence of Gd did not induce any remarkable change in the crystal properties including size, shape, porosity and surface charge (**Figure S3**). Typical Bragg peaks corresponding to FAU-type zeolite are fully preserved after ion exchange treatment (**Figure S3A**). The introduction of cations into zeolites was used to track their ability to reach the brain tumor after intravenous injection using MRI. Gd-containing zeolites were already examined as MRI contrast agents and showed no leakage of Gd outside the framework [27]. First, a Gd-FAU zeolite suspension was injected intravenously in healthy rats and blood samples were then taken at various times thereafter. Quantification of Gd-FAU zeolites in the blood was performed through the characterization of gadolinium content with ICP-MS. The blood half-life of Gd-FAU was calculated to be 12 min (**Figure 5A**).

Gd-FAU zeolites were then used to assess whether nanosized zeolites can extravasate into the brain tumors after intravenous injection. An earlier study reported that nanosized zeolites are expected to extravasate and accumulate in the tumor tissue, although they should not cross the intact blood-brain barrier [40]. To verify this assumption, dynamic T1-weighted MRI was employed to examine the distribution of zeolite nanocrystals in the brain after their intravenous administration. A hyper-signal was observed specifically inside the tumor (**Figure 5B, C, Figure S4, and supplementary movie**) while no change was observed in the healthy brain. The comparison between the T1-w images acquired before and after the injection of zeolites confirms that the zeolite nanocrystals efficiently reached the tumor and not the surrounding healthy tissue (**Figure 5B**). The maximum increase in the signal was seen 100 sec after the administration of

zeolites (**Figure 5C**). These results confirmed the precise transfer of the zeolite nanocrystals in the tumor, thus they could be evaluated as a carrier to deliver hypercapnic/hyperoxic gases.

Nanosized zeolites as gas carriers to specifically reoxygenate brain tumors

Multiparametric MRI was employed in a human GBM model to assess the functional benefits of nanosized zeolites as gas (CO₂ and O₂) carriers. Furthermore, the incorporation of gadolinium into zeolites did not modify their capacity to adsorb O₂ (**Figure S5A**). Likewise, Gd-FAU zeolites retained their ability to adsorb CO₂, while in a lower amount (3.98 to 2.28 and 3.79 to 1.36 band area/g for physisorbed and chemisorbed CO₂ respectively, **Figure S5B**).

Variations in cerebral blood volume (CBV) following an intravenous administration of zeolites loaded with CO₂ was measured and expressed as Δ CBV. Findings showed an augmentation of the CBV inside the tumor relative to the non-tumoral tissue (**Figure 6A, B**), leading to a difference of 15% between the two tissues at 15 min following the injection. When water saturated with CO₂ was used as a reference, a maximum difference of 5% of the CBV in the tumor compared to the healthy tissue was quantified (**Figure 6A, B**). Upon switching the pure CO₂ with carbogen into Gd-FAU for concurrently targeting the CBV and the tissue oxygenation, the difference of signal measured between the healthy and tumor tissues was 5.36% (**Figure 6A, C**). These results indicate that nanosized zeolites loaded with dilator gases induce vasodilatation specifically within the tumor. This contrast with our earlier investigations in which inhalation of carbogen induced a CBV increase in the healthy brain but not in the tumor [9].

The SatO₂-MRI, an imaging technique reported to precisely assess tissue hypoxia [41], was used before and after administration of the zeolites loaded with CO₂ or carbogen (Δ SatO₂). The re-oxygenation of the tumor in comparison to the healthy tissue ($\Delta\Delta$ SatO₂) was quantified (**Figure**

6A, B, C). The intravenous delivery of zeolites carrying CO₂ and carbogen increased $\Delta\Delta\text{SatO}_2$ of 6.43% and 2.07%, respectively. A further control was made by injecting zeolites (300 μl , 1 wt%) without gas loading. No augmentation of CBV or SatO₂ was found, indicating that the modifications are due to the transported gas and not to the nanosized zeolites *per se* (**Figure S6**). Furthermore, when CBV and SatO₂-MRI were quantified 1 h after injection, the selective enhancement of CBV and SatO₂ within the tumor relative to the healthy tissue was still observed. The lower effect observed with carbogen suggest that the primary effect is an increased perfusion via vasodilatory effects of CO₂ and not reoxygenation via oxygen delivery. However, the U87 GBM model used here is moderately hypoxic. [31,42]. Figure 2C shows that the delivery of oxygen by zeolites is dependent on the oxygen pressure of the environment. Therefore, the relatively high oxygen pressure in the U87-MG tumor could prevent the zeolites from releasing their oxygen payload.

We lastly evaluated if any release of CO₂ could also take place in the systemic circulation by monitoring the arterial partial pressure of CO₂ (PaCO₂) following the intravenous administration of the Gd-FAU loaded with CO₂ (**Figure 6D**). The PaCO₂ displayed a 4 mmHg increase at 10 min following the injection of CO₂-loaded zeolites (**Figure 5A**), paralleled by a minor acidification, i.e., the pH decreased from 7.53 to 7.36 (**Figure 6E**). These modifications were not observed when the control sample was used. The augmentation of the PaCO₂ could lead to a vasodilation. Therefore, dynamic BOLD-MRI was achieved to follow the variations of blood flow of large vessels, such as the venous sinus. The intravenous administration of nanosized zeolites loaded with CO₂ induced an enhancement of the BOLD signal up to $5.05 \pm 6.50\%$ as did inhalation of 5% CO₂. Administration of control sample or pure nanosized zeolites without CO₂ did not change the BOLD signal (**Figure 6F**). These data demonstrate that nanosized zeolites are

able to carry CO₂ or carbogen and enhance blood volume and oxygenation specifically within the tumor.

Conclusions

The use of functional nanoparticles has dramatically increased during the last years in the management of tumors [43,44]. In the present study, the use of nanosized zeolite particles as a specific gas carrier for glioblastoma was studied. Additionally, thanks to the presence of Gd into zeolite nanoparticles, enabling MRI tracking, the specific accumulation of nanosized zeolites in the tumor was evidenced. The nanosized zeolites loaded with CO₂ or carbogen (95% O₂ and 5% CO₂) successfully increased the blood volume and oxygenation in the tumor tissue relative to the healthy tissue (**Figure 7**).

No clinical study that evaluated targeted administration of hyperoxic/hypercapnic in glioblastoma is available. A clinical investigation has suggested that hyperbaric oxygen therapy (HBOT) may improve the efficacy of radio-chemotherapy to some extent [45]. In clinical trials, although it showed some positive results in certain types of cancer (e.g. head & neck), carbogen inhalation resulted in unsatisfactory outcomes for GBM patients [7,8]. In our previous study [9], we showed that inhalation of carbogen increased cerebral blood flow in the healthy tissue at the expense of the tumor, a phenomenon that can be attributed to the flow steal phenomenon and argues for the importance of vectorization of hyperoxic/hypercapnic gases to specifically target the tumor using zeolites. The specific delivery of hyperoxic gases has been suggested using micronsized particles [16] but their use to alleviate hypoxia in brain tumors is not satisfactory because of their large diameter disabling any entry into the tumor. The use of perfluorochemicals has also been recently discussed [46] but this strategy has not been applied to GBM.

In addition, the results from our study show that the amount of oxygen released from the zeolites is higher as the external oxygen pressure is low. Interestingly, it can be assumed that in an organism, the zeolite would keep its oxygen payload until it reaches a hypoxic region, like in GBM, where they would release the oxygen. In addition, the incorporation of other cations may improve the ability of zeolites to carry more oxygen.

Zeolites are alternative nanoparticles designed for delivery of oxygen. In addition to their stability, one of the main advantages of zeolites is their versatility. By adjusting their physicochemical properties, it is possible to add new features, such as the incorporation of cations, used in the present study to image the particles *in vivo*. In addition, heavy atoms such as gadolinium can act as radiosensitizers [12], and this could be combined with the gas delivery in a context of radiotherapy treatment. Other studies reported on the incorporation of gamma-emitter such as $^{111}\text{In}^{3+}$ via ion exchange [20]. Nanosized zeolites have been used to encapsulate and deliver siRNA and chemotherapy agents, in particular temozolomide [22]. Functionalized zeolites with antibodies were also used to target cancer cells [23]. Nanosized zeolites could simultaneously gather many features to improve the diagnosis and treatment of GB. Another important advantage of nanozeolites is their stability and limited toxicity.

In summary, the great potential of nanosized zeolites for glioblastoma is envisioned. This paves the way for the use of carbogen-loaded or oxygen loaded Gd-containing zeolite nanocrystals to the tumor, as a carrier of (i) high-Z containing elements and (ii) re-oxygenating gases, which are known to increase the efficiency of radiotherapy.

After demonstrating that nanozeolites could be used to improve tumor oxygenation, further *in vivo* studies will be performed to address their efficacy together with conventional therapies used for glioblastoma.

Acknowledgements

This work was supported by the Conseil Régional de Basse-Normandie (Projet Emergence ZEOXY), the European Union-Fonds Européen de Développement Régional (FEDER), the CNRS, the University of Caen Normandy and the Institut National du Cancer (INCA 11699).

References

- [1] D.N. Louis, A. Perry, G. Reifenberger, A. von Deimling, D. Figarella-Branger, W.K. Cavenee, H. Ohgaki, O.D. Wiestler, P. Kleihues, D.W. Ellison, The 2016 World Health Organization Classification of Tumors of the Central Nervous System: a summary, *Acta Neuropathol.* 131 (2016) 803–820. <https://doi.org/10.1007/s00401-016-1545-1>.
- [2] O.L. Chinot, W. Wick, W. Mason, R. Henriksson, F. Saran, R. Nishikawa, A.F. Carpentier, K. Hoang-Xuan, P. Kavan, D. Cernea, A.A. Brandes, M. Hilton, L. Abrey, T. Cloughesy, Bevacizumab plus Radiotherapy–Temozolomide for Newly Diagnosed Glioblastoma, *New England Journal of Medicine.* 370 (2014) 709–722. <https://doi.org/10.1056/NEJMoa1308345>.
- [3] A. Chakhoyan, J.-S. Guillamo, S. Collet, F. Kauffmann, N. Delcroix, E. Lechapt-Zalcman, J.-M. Constans, E. Petit, E.T. MacKenzie, L. Barré, M. Bernaudin, O. Touzani, S. Valable, FMISO-PET-derived brain oxygen tension maps: application to glioblastoma and less aggressive gliomas, *Sci Rep.* 7 (2017). <https://doi.org/10.1038/s41598-017-08646-y>.
- [4] K.L. Eales, K.E.R. Hollinshead, D.A. Tennant, Hypoxia and metabolic adaptation of cancer cells, *Oncogenesis.* 5 (2016) e190. <https://doi.org/10.1038/oncsis.2015.50>.
- [5] W.R. Wilson, M.P. Hay, Targeting hypoxia in cancer therapy, *Nature Reviews Cancer.* 11 (2011) 393–410. <https://doi.org/10.1038/nrc3064>.
- [6] S.M. Evans, K.W. Jenkins, H.I. Chen, W.T. Jenkins, K.D. Judy, W.-T. Hwang, R.A. Lustig, A.R. Judkins, M.S. Grady, S.M. Hahn, C.J. Koch, The Relationship among Hypoxia, Proliferation, and Outcome in Patients with De Novo Glioblastoma: A Pilot Study, *Transl Oncol.* 3 (2010) 160–169.
- [7] J.H. Kaanders, J. Bussink, A.J. van der Kogel, ARCON: a novel biology-based approach in radiotherapy, *The Lancet Oncology.* 3 (2002) 728–737. [https://doi.org/10.1016/S1470-2045\(02\)00929-4](https://doi.org/10.1016/S1470-2045(02)00929-4).
- [8] R.W.M. van der Maazen, H.O.M. Thijssen, J.H.A.M. Kaanders, A. de Koster, A. Keyser, M.J.J. Prick, J.A. Grotenhuis, P. Wesseling, A.J. van der Kogel, Conventional radiotherapy combined with carbogen breathing and nicotinamide for malignant gliomas, *Radiotherapy and Oncology.* 35 (1995) 118–122. [https://doi.org/10.1016/0167-8140\(95\)01534-N](https://doi.org/10.1016/0167-8140(95)01534-N).
- [9] A. Chakhoyan, A. Corroyer-Dulmont, M.M. Leblond, A. Gérault, J. Toutain, L. Chazaviel, D. Divoux, E. Petit, E.T. MacKenzie, F. Kauffmann, N. Delcroix, M. Bernaudin, O. Touzani, S. Valable, Carbogen-induced increases in tumor oxygenation depend on the vascular status of the tumor: A multiparametric MRI study in two rat glioblastoma models, *J. Cereb. Blood Flow Metab.* (2016). <https://doi.org/10.1177/0271678X16663947>.
- [10] H. Maeda, H. Nakamura, J. Fang, The EPR effect for macromolecular drug delivery to solid tumors: Improvement of tumor uptake, lowering of systemic toxicity, and distinct tumor

- imaging in vivo, *Advanced Drug Delivery Reviews*. 65 (2013) 71–79. <https://doi.org/10.1016/j.addr.2012.10.002>.
- [11] S.C. Baetke, T. Lammers, F. Kiessling, Applications of nanoparticles for diagnosis and therapy of cancer, *Br J Radiol*. 88 (2015) 20150207. <https://doi.org/10.1259/bjr.20150207>.
- [12] S. Kotb, A. Detappe, F. Lux, F. Appaix, E.L. Barbier, V.-L. Tran, M. Plissonneau, H. Gehan, F. Lefranc, C. Rodriguez-Lafrasse, C. Verry, R. Berbeco, O. Tillement, L. Sancey, Gadolinium-Based Nanoparticles and Radiation Therapy for Multiple Brain Melanoma Metastases: Proof of Concept before Phase I Trial, *Theranostics*. 6 (2016) 418–427. <https://doi.org/10.7150/thno.14018>.
- [13] A.R. King, C.D. Corso, E.M. Chen, E. Song, P. Bongiorno, Z. Chen, R.K. Sundaram, R.S. Bindra, W.M. Saltzman, Local DNA Repair Inhibition for Sustained Radiosensitization of High-Grade Gliomas, *Mol Cancer Ther*. 16 (2017) 1456–1469. <https://doi.org/10.1158/1535-7163.MCT-16-0788>.
- [14] J. Xie, Y. Yong, X. Dong, J. Du, Z. Guo, L. Gong, S. Zhu, G. Tian, S. Yu, Z. Gu, Y. Zhao, Therapeutic Nanoparticles Based on Curcumin and Bamboo Charcoal Nanoparticles for Chemo-Photothermal Synergistic Treatment of Cancer and Radioprotection of Normal Cells, *ACS Appl Mater Interfaces*. 9 (2017) 14281–14291. <https://doi.org/10.1021/acsami.7b02622>.
- [15] Y. Sheng, H. Nesbitt, B. Callan, M.A. Taylor, M. Love, A.P. McHale, J.F. Callan, Oxygen generating nanoparticles for improved photodynamic therapy of hypoxic tumours, *J Control Release*. 264 (2017) 333–340. <https://doi.org/10.1016/j.jconrel.2017.09.004>.
- [16] R.P. Seekell, A.T. Lock, Y. Peng, A.R. Cole, D.A. Perry, J.N. Kheir, B.D. Polizzotti, Oxygen delivery using engineered microparticles, *PNAS*. 113 (2016) 12380–12385. <https://doi.org/10.1073/pnas.1608438113>.
- [17] C. Anfray, B. Dong, S. Komaty, S. Mintova, S. Valable, Acute Toxicity of Silver Free and Encapsulated in Nanosized Zeolite for Eukaryotic Cells, *ACS Appl. Mater. Interfaces*. (2017). <https://doi.org/10.1021/acsami.7b00265>.
- [18] V. Georgieva, C. Anfray, R. Retoux, V. Valtchev, S. Valable, S. Mintova, Iron loaded EMT nanosized zeolite with high affinity towards CO₂ and NO, *Microporous and Mesoporous Materials*. 232 (2016) 256–263. <https://doi.org/10.1016/j.micromeso.2016.06.015>.
- [19] L.C.J. Thomassen, D. Napierska, D. Dinsdale, N. Lievens, J. Jammaer, D. Lison, C.E.A. Kirschhock, P.H. Hoet, J.A. Martens, Investigation of the cytotoxicity of nanozeolites A and Y, *Nanotoxicology*. 6 (2012) 472–485. <https://doi.org/10.3109/17435390.2011.587901>.
- [20] M.M. Tsotsalas, K. Kopka, G. Luppi, S. Wagner, M.P. Law, M. Schäfers, L. De Cola, Encapsulating ¹¹¹In in Nanocontainers for Scintigraphic Imaging: Synthesis, Characterization, and In Vivo Biodistribution, *ACS Nano*. 4 (2010) 342–348. <https://doi.org/10.1021/nn901166u>.
- [21] M. Tsotsalas, M. Busby, E. Gianolio, S. Aime, L. De Cola, Functionalized Nanocontainers as Dual Magnetic and Optical Probes for Molecular Imaging Applications, *Chem. Mater*. 20 (2008) 5888–5893. <https://doi.org/10.1021/cm8006183>.
- [22] O. Martinho, N. Vilaça, P.J.G. Castro, R. Amorim, A.M. Fonseca, F. Baltazar, R.M. Reis, I.C. Neves, In vitro and in vivo studies of temozolomide loading in zeolite structures as drug delivery systems for glioblastoma, *RSC Adv*. 5 (2015) 28219–28227. <https://doi.org/10.1039/C5RA03871E>.

- [23] R. Marega, E.A. Prasetyanto, C. Michiels, L. De Cola, D. Bonifazi, Fast Targeting and Cancer Cell Uptake of Luminescent Antibody-Nanozeolite Bioconjugates, *Small*. 12 (2016) 5431–5441. <https://doi.org/10.1002/sml.201601447>.
- [24] M. Zaarour, B. Dong, I. Naydenova, R. Retoux, S. Mintova, Progress in zeolite synthesis promotes advanced applications, *Microporous and Mesoporous Materials*. 189 (2014) 11–21. <https://doi.org/10.1016/j.micromeso.2013.08.014>.
- [25] S. Mintova, M. Jaber, V. Valtchev, Nanosized microporous crystals: emerging applications, *Chem. Soc. Rev.* 44 (2015) 7207–7233. <https://doi.org/10.1039/C5CS00210A>.
- [26] D.G. Seifu, T.T. Isimjan, K. Mequanint, Tissue engineering scaffolds containing embedded fluorinated-zeolite oxygen vectors, *Acta Biomaterialia*. 7 (2011) 3670–3678. <https://doi.org/10.1016/j.actbio.2011.06.010>.
- [27] E. Csajbók, I. Bányai, L. Vander Elst, R.N. Muller, W. Zhou, J.A. Peters, Gadolinium(III)-loaded nanoparticulate zeolites as potential high-field MRI contrast agents: relationship between structure and relaxivity, *Chemistry*. 11 (2005) 4799–4807. <https://doi.org/10.1002/chem.200500039>.
- [28] H. Awala, J.-P. Gilson, R. Retoux, P. Boullay, J.-M. Goupil, V. Valtchev, S. Mintova, Template-free nanosized faujasite-type zeolites, *Nat Mater*. 14 (2015) 447–451. <https://doi.org/10.1038/nmat4173>.
- [29] M. Bernaudin, A. Bellail, H.H. Marti, A. Yvon, D. Vivien, I. Duchatelle, E.T. Mackenzie, E. Petit, Neurons and astrocytes express EPO mRNA: oxygen-sensing mechanisms that involve the redox-state of the brain, *Glia*. 30 (2000) 271–278.
- [30] M.M. Leblond, E.A. Pérès, C. Helaine, A.N. Gérault, D. Moulin, C. Anfray, D. Divoux, E. Petit, M. Bernaudin, S. Valable, M2 macrophages are more resistant than M1 macrophages following radiation therapy in the context of glioblastoma, *Oncotarget*. 8 (2017) 72597–72612. <https://doi.org/10.18632/oncotarget.19994>.
- [31] A. Corroyer-Dulmont, E.A. Pérès, E. Petit, L. Durand, L. Marteau, J. Toutain, D. Divoux, S. Roussel, E.T. MacKenzie, L. Barré, M. Bernaudin, S. Valable, Noninvasive assessment of hypoxia with 3-[18F]-fluoro-1-(2-nitro-1-imidazolyl)-2-propanol ([18F]-FMISO): a PET study in two experimental models of human glioma, *Biological Chemistry*. 394 (2013). <https://doi.org/10.1515/hsz-2012-0318>.
- [32] S. Komaty, C. Anfray, M. Zaarour, H. Awala, V. Ruaux, S. Valable, S. Mintova, A Facile Route toward the Increase of Oxygen Content in Nanosized Zeolite by Insertion of Cerium and Fluorinated Compounds, *Molecules*. 23 (2018). <https://doi.org/10.3390/molecules23020037>.
- [33] N. Vilaça, R. Amorim, A.F. Machado, P. Parpot, M.F.R. Pereira, M. Sardo, J. Rocha, A.M. Fonseca, I.C. Neves, F. Baltazar, Potentiation of 5-fluorouracil encapsulated in zeolites as drug delivery systems for in vitro models of colorectal carcinoma, *Colloids and Surfaces B: Biointerfaces*. 112 (2013) 237–244. <https://doi.org/10.1016/j.colsurfb.2013.07.042>.
- [34] S. Komaty, A. Daouli, M. Badawi, C. Anfray, M. Zaarour, S. Valable, S. Mintova, Incorporation of trivalent cations in NaX zeolite nanocrystals for the adsorption of O₂ in the presence of CO₂, *Phys. Chem. Chem. Phys.* 22 (2020) 9934–9942. <https://doi.org/10.1039/D0CP00111B>.
- [35] M.Y. Koh, G. Powis, Passing the baton: The HIF switch, *Trends Biochem Sci*. 37 (2012) 364–372. <https://doi.org/10.1016/j.tibs.2012.06.004>.

- [36] H. Kempf, M. Bleicher, M. Meyer-Hermann, Spatio-Temporal Dynamics of Hypoxia during Radiotherapy, *PLOS ONE*. 10 (2015) e0133357. <https://doi.org/10.1371/journal.pone.0133357>.
- [37] T. Le Gall, V. Polard, M. Rousselot, A. Lotte, M. Raouane, P. Lehn, P. Opolon, E. Leize, E. Deutsch, F. Zal, T. Montier, In vivo biodistribution and oxygenation potential of a new generation of oxygen carrier, *Journal of Biotechnology*. 187 (2014) 1–9. <https://doi.org/10.1016/j.jbiotec.2014.07.008>.
- [38] N. Bayat, V.R. Lopes, J. Schölermann, L.D. Jensen, S. Cristobal, Vascular toxicity of ultra-small TiO₂ nanoparticles and single walled carbon nanotubes in vitro and in vivo, *Biomaterials*. 63 (2015) 1–13. <https://doi.org/10.1016/j.biomaterials.2015.05.044>.
- [39] P.A. Chiarelli, R.A. Revia, Z.R. Stephen, K. Wang, M. Jeon, V. Nelson, F.M. Kievit, J. Sham, R.G. Ellenbogen, H.-P. Kiem, M. Zhang, Nanoparticle Biokinetics in Mice and Nonhuman Primates, *ACS Nano*. 11 (2017) 9514–9524. <https://doi.org/10.1021/acsnano.7b05377>.
- [40] A. Karageorgis, S. Dufort, L. Sancey, M. Henry, S. Hirsjärvi, C. Passirani, J.-P. Benoit, J. Gravier, I. Texier, O. Montigon, M. Benmerad, V. Siroux, E.L. Barbier, J.-L. Coll, An MRI-based classification scheme to predict passive access of 5 to 50-nm large nanoparticles to tumors, *Scientific Reports*. 6 (2016). <https://doi.org/10.1038/srep21417>.
- [41] T. Christen, B. Lemasson, N. Pannetier, R. Farion, C. Segebarth, C. Rémy, E.L. Barbier, Evaluation of a quantitative blood oxygenation level-dependent (qBOLD) approach to map local blood oxygen saturation, *NMR Biomed*. 24 (2011) 393–403. <https://doi.org/10.1002/nbm.1603>.
- [42] S. Valable, A. Corroyer-Dulmont, A. Chakhoyan, L. Durand, J. Toutain, D. Divoux, L. Barré, E.T. MacKenzie, E. Petit, M. Bernaudin, O. Touzani, E.L. Barbier, Imaging of brain oxygenation with magnetic resonance imaging: A validation with positron emission tomography in the healthy and tumoural brain, *J. Cereb. Blood Flow Metab*. (2016). <https://doi.org/10.1177/0271678X16671965>.
- [43] C. Chen, Y. Liu, H. Wang, G. Chen, X. Wu, J. Ren, H. Zhang, Y. Zhao, Multifunctional Chitosan Inverse Opal Particles for Wound Healing, *ACS Nano*. 12 (2018) 10493–10500. <https://doi.org/10.1021/acsnano.8b06237>.
- [44] J. Wang, G. Chen, Z. Zhao, L. Sun, M. Zou, J. Ren, Y. Zhao, Responsive graphene oxide hydrogel microcarriers for controllable cell capture and release, *Sci. China Mater*. 61 (2018) 1314–1324. <https://doi.org/10.1007/s40843-018-9251-9>.
- [45] L. Huang, W. Boling, J.H. Zhang, Hyperbaric oxygen therapy as adjunctive strategy in treatment of glioblastoma multiforme, *Med Gas Res*. 8 (2018) 24–28. <https://doi.org/10.4103/2045-9912.229600>.
- [46] Z. Zhou, B. Zhang, H. Wang, A. Yuan, Y. Hu, J. Wu, Two-stage oxygen delivery for enhanced radiotherapy by perfluorocarbon nanoparticles, *Theranostics*. 8 (2018) 4898–4911. <https://doi.org/10.7150/thno.27598>.
- [47] D.W. McNeas, B.J. Ponzio, R.W. Lewis, F.J. Stein, R.F. Sis, B.M. Levy, Hematology of common marmosets (*Callithrix jacchus*), *Primates*. 23 (1982) 145–150. <https://doi.org/10.1007/BF02381447>.
- [48] D.W. McNeas, R.W. Lewis, B.J. Ponzio, R.F. Sis, F.J. Stein, Blood chemistry of the common marmoset (*Callithrix jacchus*) maintained in an indoor-outdoor environment: Primate comparisons, *Primates*. 25 (1984) 103–109. <https://doi.org/10.1007/BF02382300>.

Author Contributions and competing interests

Author contribution: CA, SK, ACD, MZ, CH, HO, CA, JT, KG, SM, SV performed the experiments and analyzed the data. CA, EP, VV, OT, SM and SV interpreted the data. CA, KB, OT, SM and SV contributed to conception and design. CA, OT, SM and SV approved the final version.

Data availability

The datasets generated during and/or analyzed during the current study are available from the corresponding author on reasonable request.

Figure 1. (1.5-column fitting image)

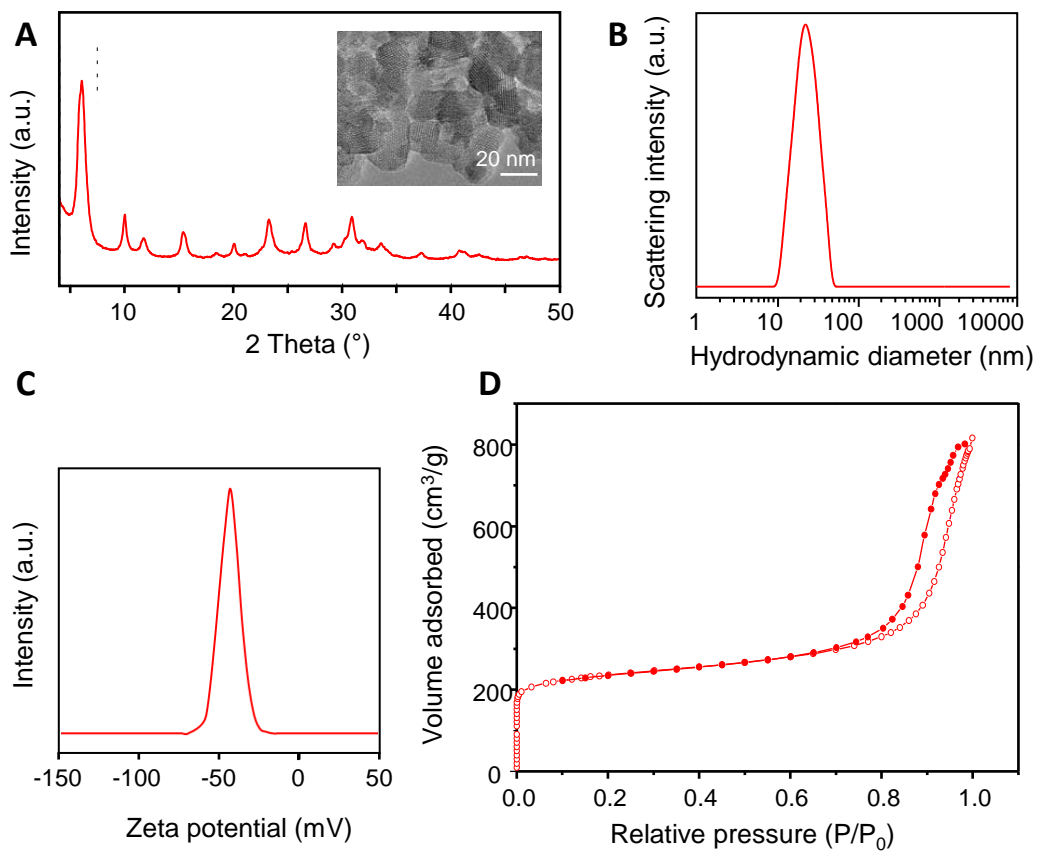


Figure 2. (1.5 fitting image)

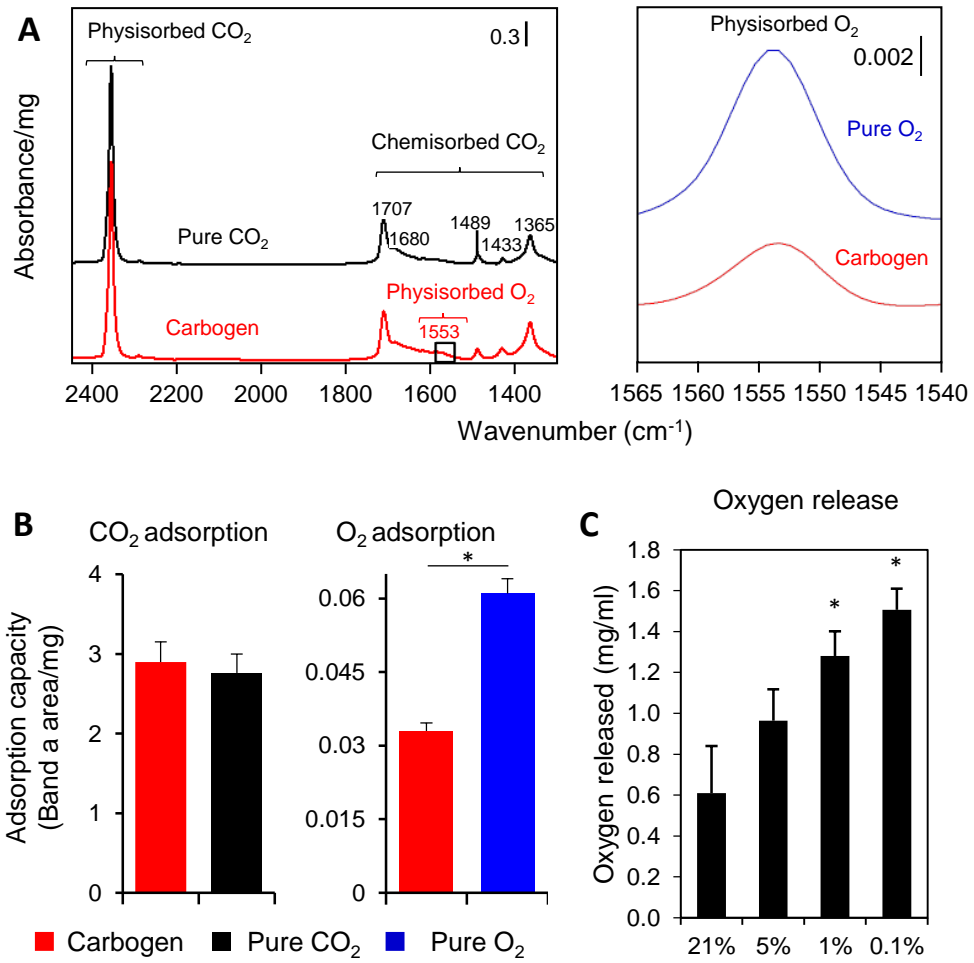


Figure 3. (2-column fitting image)

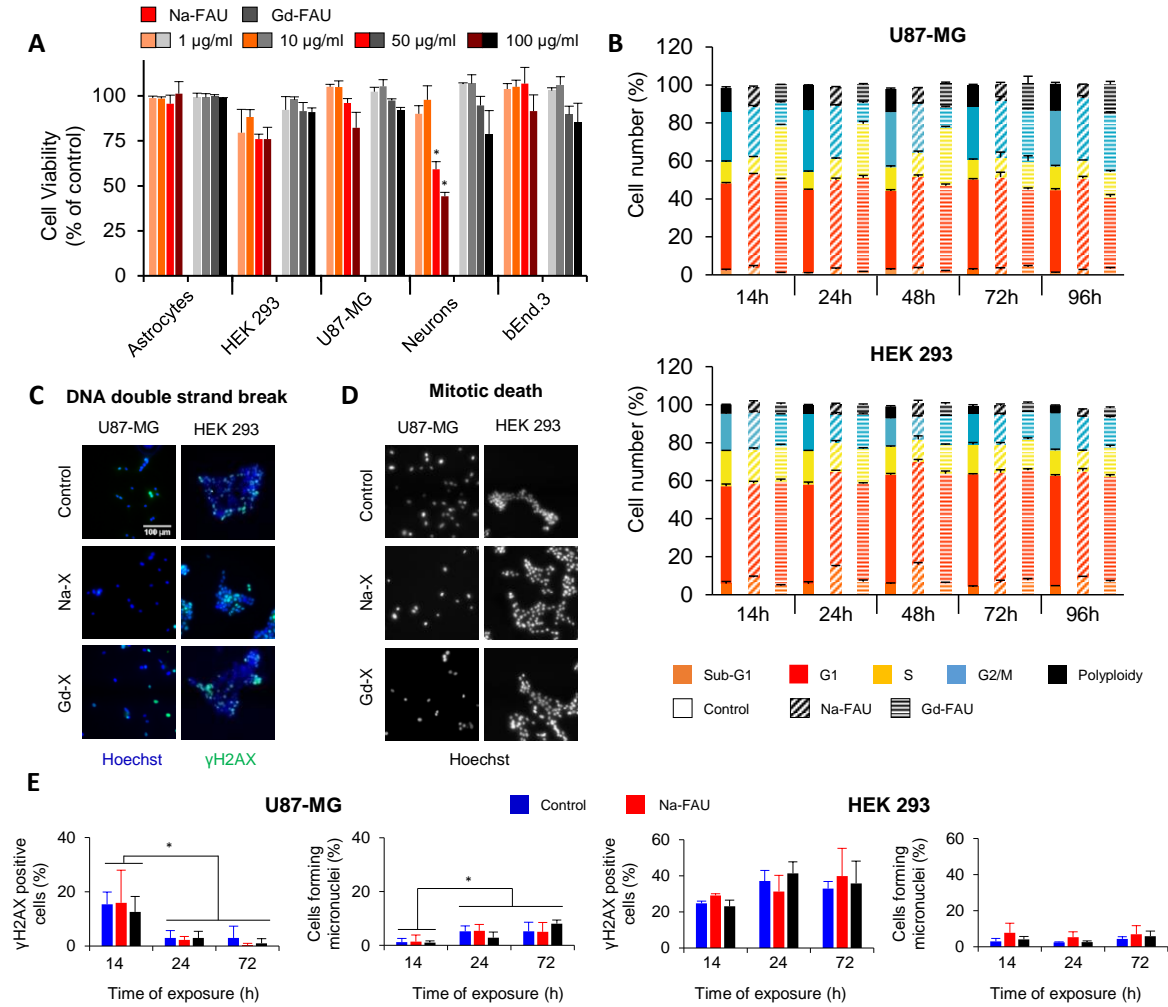


Figure 4. (2-column fitting image)

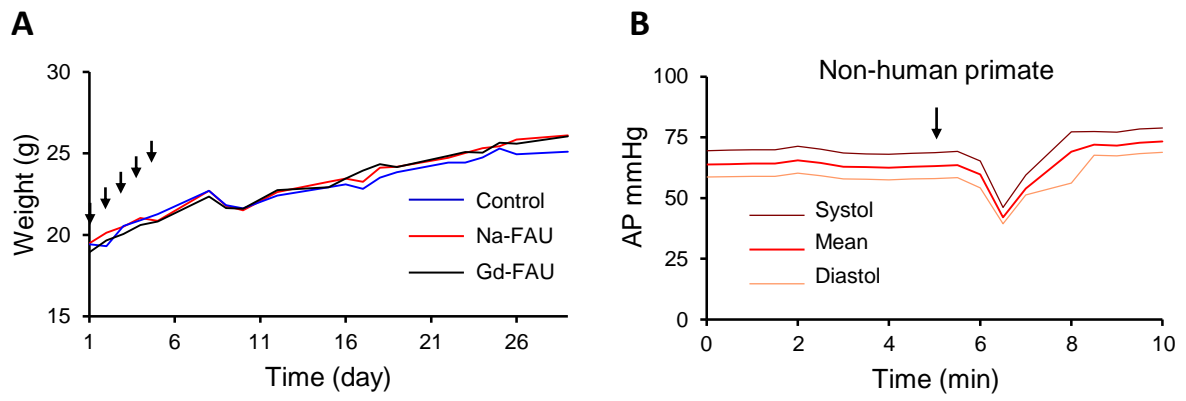


Figure 5. (2-column fitting image)

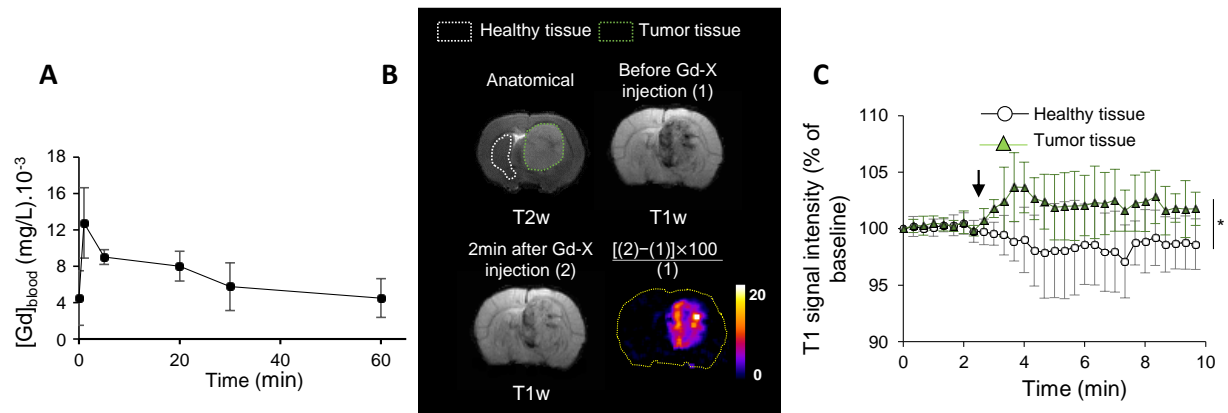


Figure 6. (2-column fitting image)

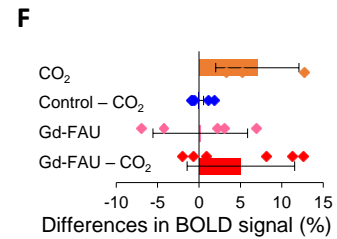
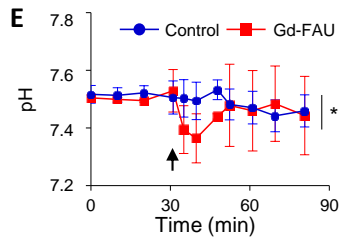
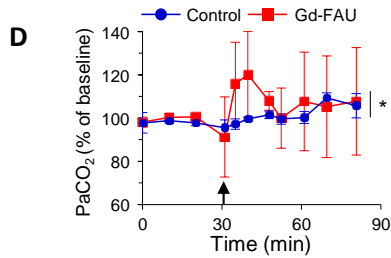
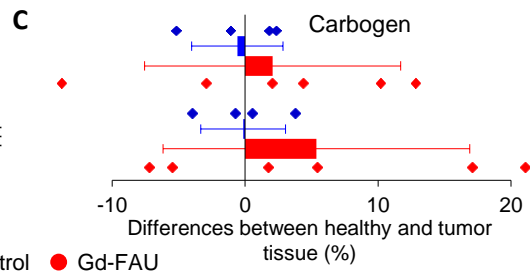
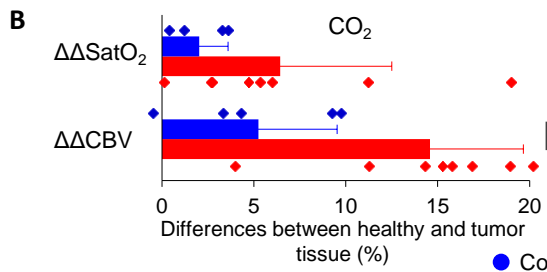
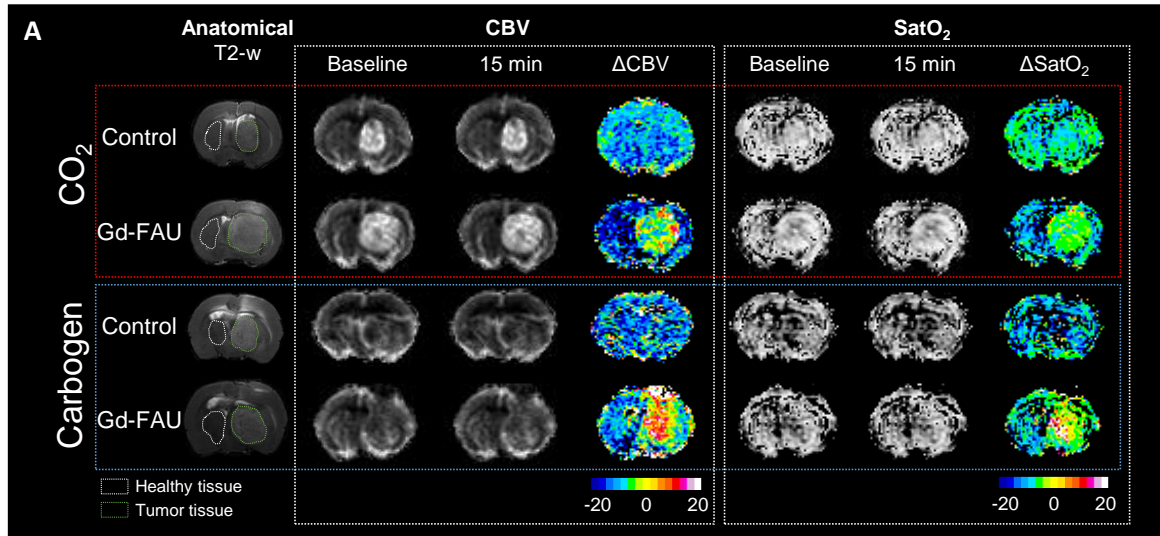


Figure 7. (1.5 column fitting image)

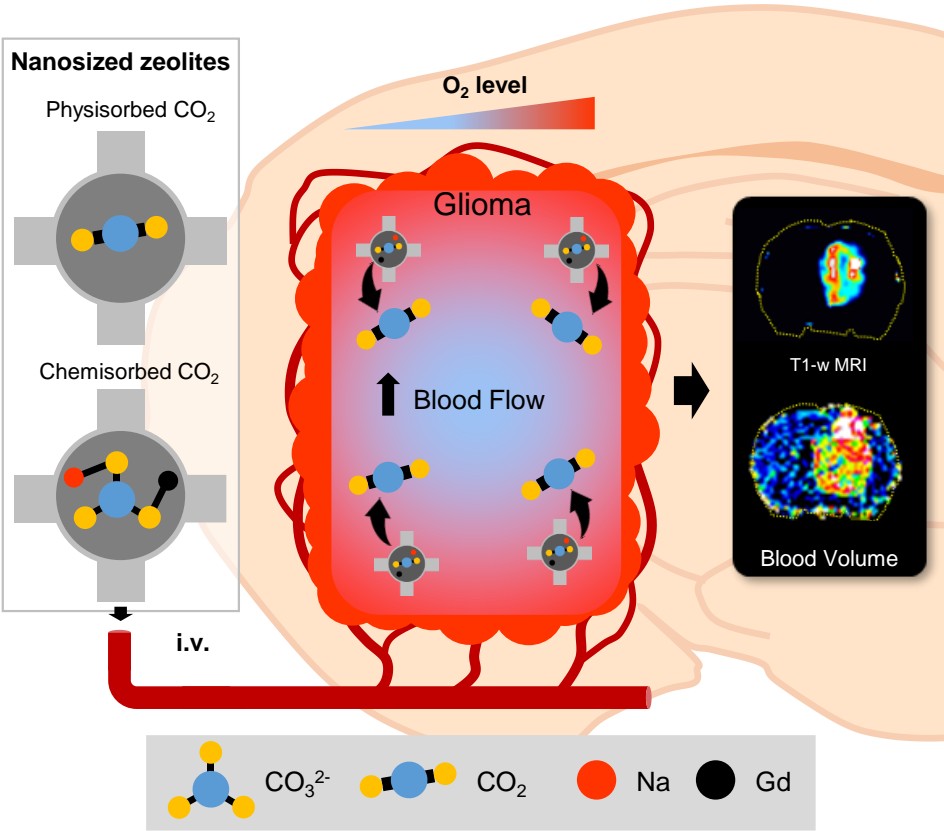


Figure Captions and Tables

Figure 1. Main physicochemical properties of zeolite nanocrystals. (A) XRD patterns (*Inset: TEM pictures*). (B) Dynamic Light Scattering (DLS) curves. (C) Zeta potential curves. (D) Nitrogen adsorption/desorption isotherms (full symbols refer to adsorption, open symbols refer to desorption).

Figure 2. Nanosized zeolites are able to adsorb and release gases. (A) FTIR spectra of physisorbed and chemisorbed CO₂ under delivery of carbogen and pure CO₂ and physisorbed oxygen under delivery of carbogen and pure O₂ on Na-FAU zeolites. (B) Adsorption capacity of CO₂ using carbogen or pure CO₂ and O₂ using carbogen or pure O₂ (*p<0.05) Mean ± s.d., n=3/condition. (C) Quantification of oxygen released from zeolites in aqueous solution (phosphate buffered saline) (*p<0.05 vs 21%). Mean ± s.d., n=3/condition.

Figure 3. Zeolite nanocrystals display no sign of toxicity *in vitro*. (A) Astrocytes, neurons, U87-MG, HEK 293 and bEnd.3 cells viability following a 48 h exposure to nanosized zeolites. Mean ± s.d., n=3/condition (*p<0.05 vs control; ANOVA and HSD Tuckey). (B) Cell cycle analysis by flow cytometry. Quantification of U87-MG and HEK 293 cells distribution in different phases of cell cycle after different times of exposure to 100 µg/ml of zeolites or water as a control. Mean ± s.d., n=3/time point. (C, D) Representative photographs of DNA double-strand breaks identified with γH2AX immunostaining (C) and micronuclei formation identified with Hoechst 33342 staining (D) on U87-MG and HEK 293 cells, 14 h after exposure to 100 µg/ml of zeolites. (E) Quantification after 14, 24 or 72 h exposure to 100 µg/ml of zeolites. Mean ± s.d., n=3/condition (*p<0.001; ANOVA and HSD Tuckey).

Figure 4. Evaluation of toxicity of nanosized zeolites *in vivo*. (A) Weight curves of mice following intraperitoneal injections of Na-FAU and Gd-FAU zeolites or water as a control during 5 consecutive days (represented with arrows). Mean, 4 mice per group. (B) Arterial pressure (AP) of a marmoset after i.v. injection of nanosized Gd-FAU zeolite carrying CO₂ (arrow indicates the time of injection). Representative example from 3 independent experiments.

Figure 5. Bio-distribution of nanosized zeolites in rats. (A) Quantification of gadolinium content in the blood versus time after i.v. injection of Gd-FAU (300 µl, 1 wt%). Mean ± s.d., 4 independent experiments. (B) Representative T1-w images acquired before (1) or two min after (2) i.v. administration of Gd-FAU (300 µl, 1 wt%); T2w image (left) and a map of the differences between the two T1w images (right). (C) Quantification of the normalized T1w signal intensity in the healthy and the tumor tissue. Baseline is the measurement of T1w signal carried out before injection and arrow refers to the time of injection. Mean ± s.d., 5 independent experiments. (*p<0.0001; two-way ANOVA). See also the video in Supplementary Information.

Figure 6. Nanosized zeolites carrying hyperoxic gases influence CBV and SatO₂ in the tumour. (A) Representative T2-w anatomic images, CBV and SatO₂ maps obtained before and 15 min after i.v. injection of nanosized Gd-FAU zeolite (300 µl, 1 wt%) carrying CO₂ or carbogen and the corresponding differences between the two maps (Δ CBV and Δ SatO₂, respectively). Control consisted of injection of H₂O saturated with CO₂ or carbogen. (B) and (C) Quantification of the differences of Δ CBV and Δ SatO₂ (%) between the healthy and the tumor tissue ($\Delta\Delta$ CBV and $\Delta\Delta$ SatO₂, respectively). Mean ± s.d., n=5 for control group; n=8 for Gd-FAU with CO₂ group; n=5 for Gd-FAU with carbogen group (***p<0.001; ANOVA). (D) Evolution of the arterial pressure of CO₂ (PaCO₂) expressed in percentage of baseline and (E) pH in the blood of healthy Wistar rats following injection of Gd-FAU (300 µl, 1 wt%) carrying

CO₂ or control. Baseline refers to measurement of PaCO₂ performed before injection and arrow indicates the time of injection. Mean ± s.d., n=5 per group (*p<0.05; two-way ANOVA). (F) Differences in Blood Oxygen Level Dependent (BOLD) signal measured in the venous sinus of healthy Wistar rats before and 3 min after an i.v. injection of Gd-FAU (300 µl, 1 wt%) carrying CO₂, or control or Gd-X without CO₂ or breathing of 5% of CO₂. Mean ± s.d., n=6 for Gd-FAU – CO₂ group; n=5 for Gd-FAU group; n=4 for control – CO₂ group; n=3 for inhalation of 5% CO₂ group.

Figure 7. Nanosized zeolites are used as a specific hyperoxic gases carrier, in which they act as a vasoactive agent to increase both the blood and the oxygen supply for reoxygenation of glioblastoma. Nanosized zeolites do not cross the intact blood brain barrier, resulting in an increase in cerebral blood volume/oxygenation specifically in the tumor as compared to the healthy brain. Moreover, Gd cations introduced in the zeolite nanoparticles enable the tracking of the particles into the tumor.

Table 1. Effects of Na-FAU zeolites on the marmoset.

<i>Parameters to be tested</i>	<i>Reference range</i>	<i>Baseline Day (-7)</i>	<i>Injection Day (0)</i>	<i>One week after injection Day (+7)</i>
RBC (x10 ⁶)/mm ³	4.8-8.6 [47]	5.1	5.8	5
Hemoglobin (g %)	10.5-19.6 [47]	11.7	13.7	10.9
Hematocrit (%)	30-6 [47]	38.7	44.3	37.5
Platelets (x10 ³ /mm ³)	490 [47]	560	680	610
Monocytes (%)	0-1 [47]	1.7	0.4	1.2
Eosinophiles (%)	0-5 [47]	0.4	0.6	0.7

Basophiles (%)	0-4 [47]	0.5	1.2	1.7
Creatinine (mg/L)	0.4-11.1 [48]	8.3	5.5	5
Transaminase GOT/ASAT (UI/L)	12-228.9 [48]	68	85	89

Supplementary Data

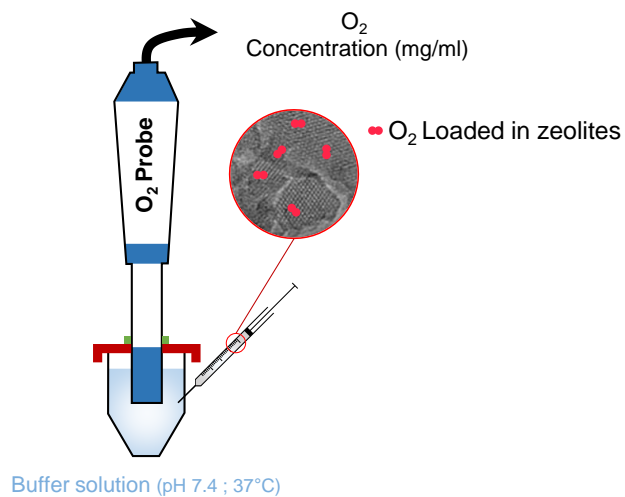


Figure S1. Schematic representation of the experimental setup used for studying the release of oxygen from zeolites in aqueous and hypoxic conditions.

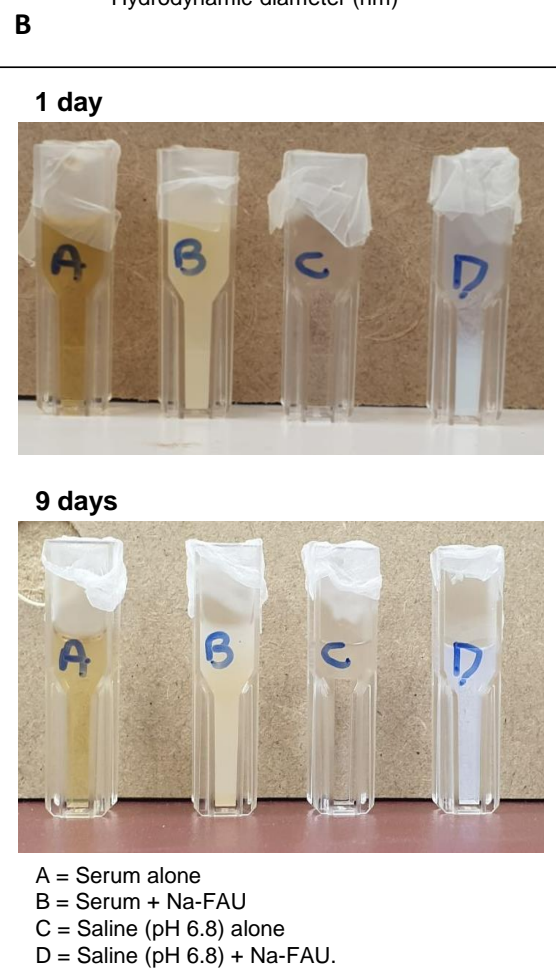
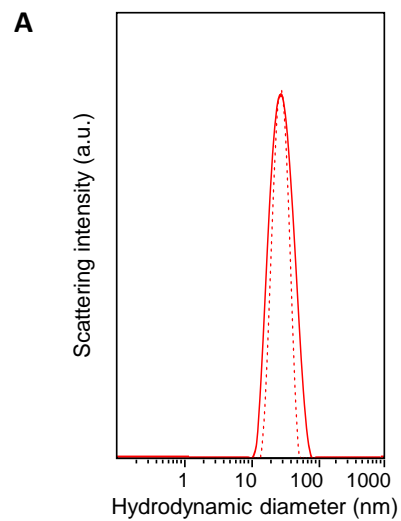


Figure S2. Nanosized zeolites remain stable in serum and at low pH. (A) Dynamic Light Scattering (DLS) curves of as prepared Na-X zeolite in water (bold) or serum (dot) suspensions.

(B) The appearance of samples of Na-FAU zeolites in serum and saline with a pH of 6.8 over time.

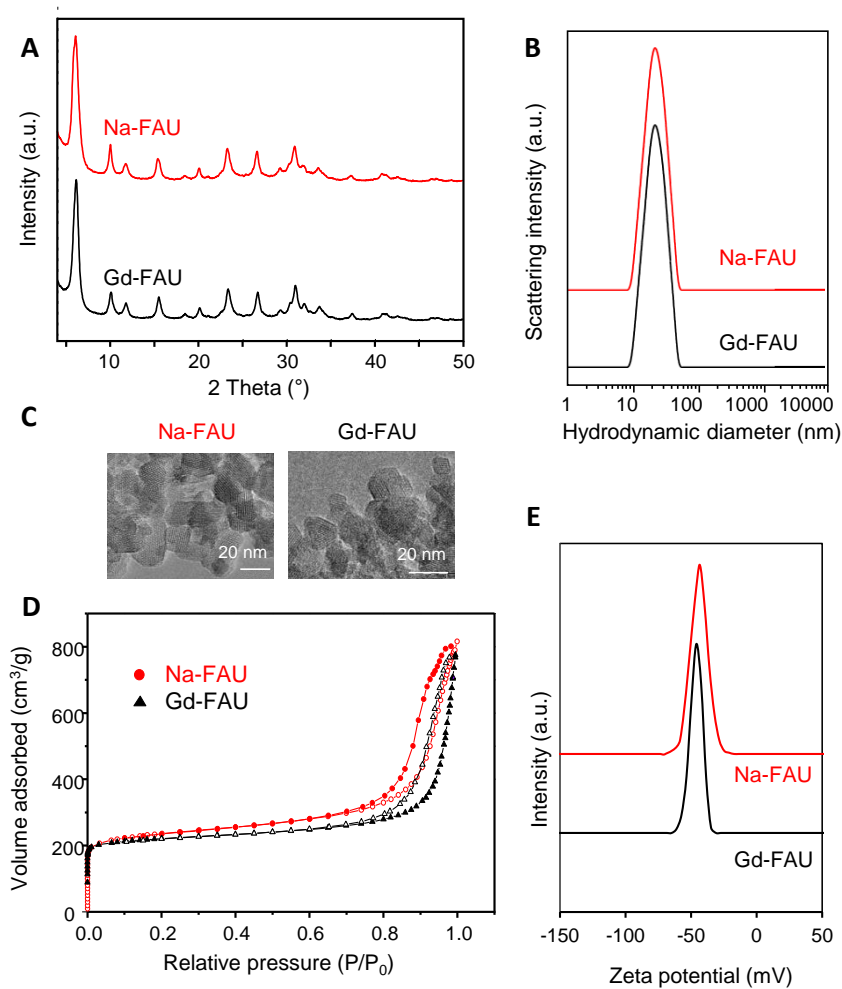


Figure S3. Comparative physicochemical properties of Na-FAU and Gd-FAU. (A) XRD patterns. (B) Dynamic Light Scattering (DLS) curves. (C) TEM pictures. (D) Nitrogen adsorption/desorption isotherms (full symbols refer to adsorption, open symbols refer to desorption). (E) Zeta potential curves.

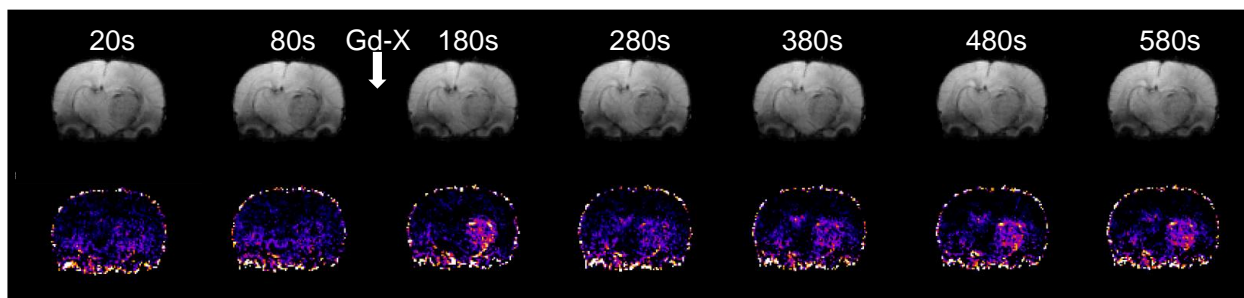


Figure S4. Gd-FAU zeolites reach the tumor. T1-w images of a rat brain acquired during an intravenous injection of a Gd-FAU suspension. The injection started at 120 s. Map of the differences of signal between the first T1-w image and the following images. See also supplementary movie.

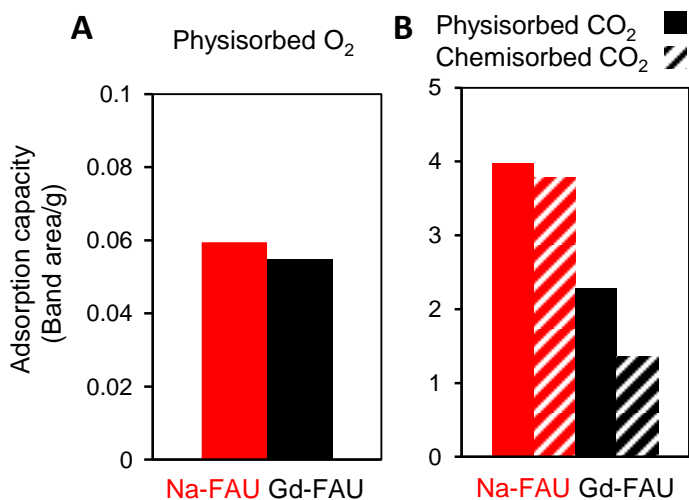


Figure S5. O₂ and CO₂ adsorption by Gd-FAU zeolites. (A) Physisorbed O₂ (measured at -196 °C) and (B) physisorbed and chemisorbed CO₂ (measured at 25 °C) on nanosized zeolites under delivery of pure CO₂ and O₂.

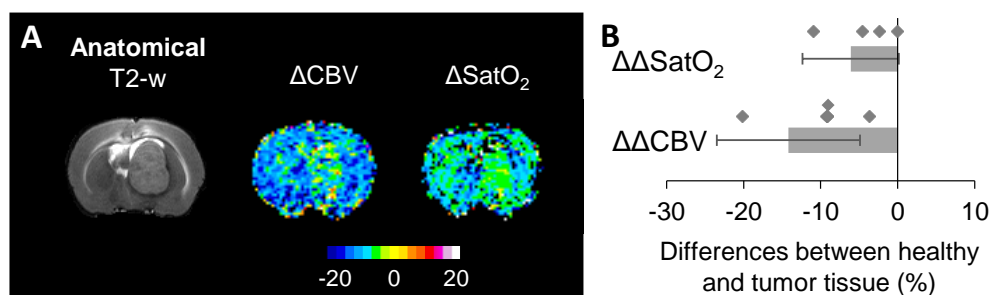


Fig. S6. Effect of empty zeolites on CBV. (A) Representative T2-w anatomic image, CBV and SatO₂ maps of the differences of signal (Δ CBV and Δ SatO₂, respectively) before and 15 min after i.v. injection of Gd-FAU (300 μ l, 1 wt%). (B) Quantification of the differences of Δ CBV and Δ SatO₂ (%) between the healthy and the tumour tissue ($\Delta\Delta$ CBV and $\Delta\Delta$ SatO₂, respectively). Mean \pm s.d. and dot-plot, n=4.

Table S1. Summary of the main characteristics of nanosized FAU-X.

	Chemical composition (wt%)				Size	Zeta potential
	Si (wt%)	Al (wt%)	Na (wt%)	Gd (wt%)		
Na-FAU	18.10	14.59	13.41	0	10-30 nm	-38mV
Gd-FAU	16.62	12.59	6.71	1.24	10-30 nm	-37.7 mV

Table S2. BET specific surface area (S_{BET}), micropore volume (V_{mic}) and total pore volume (V_{total}) of as prepared (Na-FAU) and gadolinium ion-exchanged (Gd-FAU) zeolite samples based on N₂ adsorption measurements.

Samples	S_{BET} ($\text{m}^2 \cdot \text{g}^{-1}$)	V_{mic} ($\text{cm}^3 \cdot \text{g}^{-1}$)	V_{total} ($\text{cm}^3 \cdot \text{g}^{-1}$)

Na-FAU	777	0.29	1.26
Gd-FAU	738	0.27	1.25

Table S3. Assignment of FTIR bands: adsorption of O₂, CO₂, and carbogen by zeolite samples.

IR band	Nature	Species
1553 cm ⁻¹	Physisorbed	O ₂
2346 cm ⁻¹	Physisorbed	CO ₂
1707 cm ⁻¹		Bridged carbonate bidentate
1680 cm ⁻¹		Bridged carbonate bidentate
1621 cm ⁻¹		Monodentate carbonate
1584 cm ⁻¹	Chemisorbed	Carbonate
1489 cm ⁻¹		Bidentate carbonate
1433 cm ⁻¹		Bidentate carbonate
1365 cm ⁻¹		Bridged carbonate bidentate

Movies S1. Gd-FAU zeolites have the capacity to reach the tumor.